robotics

MDPI

Article

An Aircraft-Manipulator System for Virtual Flight Testing of Longitudinal Flight Dynamics

Ademayowa A. Ishola [1,*], James F. Whidborne [1] and Gilbert Tang [2]

[1] Centre for Aeronautics, Cranfield University, Cranfield MK43 0AL, UK; j.f.whidborne@cranfield.ac.uk
[2] Centre for Robotics and Assembly, Cranfield University, Bedfordshire MK43 0AL, UK; g.tang@cranfield.ac.uk
* Correspondence: ademayowa.ishola@cranfield.ac.uk

Abstract: A virtual flight test is the process of flying an aircraft model inside a wind tunnel in a manner that replicates free-flight. In this paper, a 3-DOF aircraft-manipulator system is proposed that can be used for longitudinal dynamics virtual flight tests. The system consists of a two rotational degrees-of-freedom manipulator arm with an aircraft wind tunnel model attached to the third joint. This aircraft-manipulator system is constrained to operate for only the longitudinal motion of the aircraft. Thus, the manipulator controls the surge and heave of the aircraft whilst the pitch is free to rotate and can be actively controlled by means of an all-moving tailplane of the aircraft if required. In this initial study, a flight dynamics model of the aircraft is used to obtain dynamic response trajectories of the aircraft in free-flight. A model of the coupled aircraft-manipulator system developed using the Euler method is presented, and PID controllers are used to control the manipulator so that the aircraft follows the free-flight trajectory (with respect to the air). The inverse kinematics are used to produce the reference joint angles for the manipulator. The system is simulated in MATLAB/Simulink and a virtual flight test trajectory is compared with a free-flight test trajectory, demonstrating the potential of the proposed system for virtual flight tests.

Keywords: flight dynamics; aircraft manipulator; wind tunnel test; simulation; robot manipulator; virtual flight test

check for updates

Citation: Ishola, A.A.; Whidborne, J.F.; Tang, G. An Aircraft-Manipulator System for Virtual Flight Testing of Longitudinal Flight Dynamics. *Robotics* **2024**, *13*, 179. https://doi.org/10.3390/robotics13120179

Academic Editor: Aman Behal

Received: 18 October 2024
Revised: 6 December 2024
Accepted: 10 December 2024
Published: 15 December 2024

Copyright: © 2024 by the authors. Licensee MDPI, Basel, Switzerland. This article is an open access article distributed under the terms and conditions of the Creative Commons Attribution (CC BY) license (https://creativecommons.org/licenses/by/4.0/).

1. Introduction

Wind tunnel testing is a well-established experimental method used in aircraft analysis, and the study of fundamental flight physics and aerodynamics. While most wind tunnel experiments use static models, dynamic wind tunnel testing is useful for examining non-steady aerodynamics [1] as well as for investigating flight dynamics, especially in nonlinear flight regimes, such as those involving high angles of attack, unsteady aerodynamics, spin, and upset recovery. It is also useful for identifying aerodynamic and flight dynamic parameters [2]. For a review, see Huang and Wang [3]. However, there is also a longstanding ambition of wind tunnel testing to be able to 'fly' an aircraft inside a wind tunnel [3]. This is a challenging ambition that has limited the experience to a few very large facilities and to a few specific flight regimes. In particular, spin testing in vertical tunnels has been performed for many decades [4] and is a continuous area of interest [5].

A capability to fly the aircraft inside a wind tunnel can be seen as part of a "virtual flight testing" process [6]. Huang and Wang [3] give a definition of virtual flight testing as "flight" in a tunnel with constraints on the three translational Degrees Of Freedom (DOF). Three-rotational DOF dynamic wind tunnel testing and virtual flight testing has become fairly common over the last decade [7–13]. Recently, Tai proposed extending virtual flight testing to 4-DOF [14], but both 4- and 5-DOF dynamic wind tunnel testing have been successfully performed for some time [15–19].

Manipulators have often been proposed to improve wind tunnel experiments for various reasons, such as to provide dynamic response so that unsteady aerodynamic effects

can be investigated. For example, Asai et al. [20] developed a 2-DOF passive robot model to allow for the lateral motion of a delta wing , and Wei et al. [21] developed a 3-DOF manipulator actuated based on commands sent to the corresponding motor for variable angles of pitch, roll, and yaw. Other passive devices include an unforced pitch-axis, a 1-DOF dynamic wind tunnel test rig [22], and a 3-DOF dynamic wind tunnel test apparatus consisting of a momentum arm attached to a rigid frame [23], which allowed rotation about a gimbal for pitch and yaw with a wrist designed for roll.

Pattinson et al. suggested the use of a robotics framework with advanced capabilities in wind tunnels [24] but did not develop the idea in their paper. Some active controlled manipulator systems have been used for wind tunnel testing. For example, cable-based manipulators (to reduce interference effects) have been proposed and investigated, for example, in [25,26]. Another example is the use of a 6-DOF manipulator as part of a captive trajectory simulation system operating inside the trisonic blowdown wind tunnel facilities at the National Research Council in Canada [27]. But it appears that using a manipulator to reproduce natural flight response in a wind tunnel ha0s never been attempted. Hence, this paper proposes an aircraft-manipulator system (AMS) that performs just that. The system has a 2-DOF manipulator connected to an aircraft model that is free to pitch, which, as we show in simulation, can replicate longitudinal free-flight in a wind tunnel and, hence, can be used for virtual flight testing. A schematic of the manipulator sited in a wind tunnel is shown in Figure 1. The manipulator provides the translational variation in the wind tunnel, while the aircraft is free to pitch according to the aerodynamic forces it experiences.

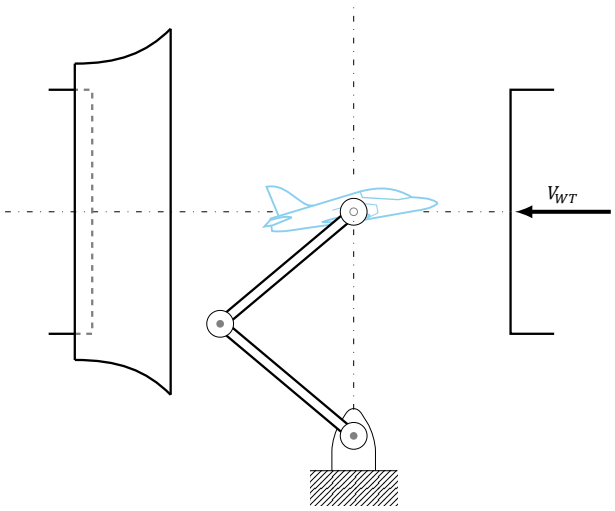


Figure 1. Schematic of the aircraft-manipulator system sited in the working section of an open-section wind tunnel (not to scale). The wind tunnel airspeed is shown as V_{WT}.

The motion of an aircraft is determined by its flight dynamics, the analysis of which is important for determining not only the stability of the aircraft, but also for the handling qualities, that is, how easy it is for the pilot to control the aircraft. Classical configuration, rigid-body, fixed-wing aircraft are usually modelled with 6-DOF (roll, pitch, yaw, surge, sway, heave) using the Newton–Euler equations, and following steady-state analysis (or 'trim'), the equations are often linearised so that modal analysis can be performed. The longitudinal dynamics (pitch, surge, heave) are fairly well decoupled from the lateral dynamics (roll, yaw, sway), and these are controlled, and analysed, separately. The longitudinal dynamics are typically controlled with an elevator and with the engine thrust, while the lateral dynamics by the ailerons and rudder. The longitudinal dynamics are typically characterised by two modes, namely the the high-frequency *short period mode* and the low-frequency *phugoid mode* e.g., [28]. There are several useful texts on flight dynamics, for example, [28–30].

The aircraft used for the modelling of the proposed AMS is based on a 1/12th scaled BAe Hawk aircraft that has been used in a 4-DOF dynamic rig at Cranfield University for parameter identification [2,15,16,19]. In that rig, the aircraft is free to pitch, roll, yaw, and heave; and the control of the aircraft is enacted by the classical elevator, rudder, and aileron moving surfaces [19]. However, the surge motion is constrained, thus limiting the virtual flight, because the velocity in the incident wind direction cannot be increased (unless the wind tunnel speed were increased), and so the aircraft lacks a controlled propulsion system and kinetic energy cannot be injected into the system. Thus, the phugoid mode cannot be accurately reproduced with the Cranfield University's 4-DOF dynamic rig. Note also that the phugoid mode in this rig can be very unstable because the airspeed decreases as the model approaches the tunnel walls, and so the lift reduces as the aircraft descends and the aircraft accelerates towards the lower tunnel wall.

In this paper, we demonstrate the feasibility of the proposed AMS system by means of simulation. A flight dynamics model of the 1/12th scaled BAe Hawk is used to generate a free-flight trajectory that excites both the short period mode and the phugoid. By an inversion of the AMS kinematics, the references for the manipulator joint angles for a wind tunnel flight are obtained. From a model of the dynamics and aerodynamics of the AMS system, the wind tunnel flight is simulated and the responses are analysed. As well as for determining aerodynamic relationships, it is envisaged that the system can be used for testing flight control laws and handling qualities. It could also be used as an educational demonstrator to show the longitudinal dynamics. Note that the aircraft-manipulator concept was originally proposed in a presentation [31], but simulations were not performed. Note also that a summary of some other simulation results from the AMS model were presented recently [32] in an extended abstract.

The nonlinear longitudinal flight dynamics of the BAe Hawk aircraft model in free-flight are presented in Section 2. Section 3 presents a nonlinear model of the proposed AMS, including the inverse kinematics, the AMS dynamics, and a PID controller for the control of the manipulator joints. Simulation results of a test trajectory are presented in Section 4, both the short period mode of the longitudinal response and low-frequency phugoid response mode. Simulation plots for free-flight trajectories and the controlled aircraft-manipulator trajectories are evaluated, and the results demonstrate the potential of the system. The potential of the system for virtual flight tests in a wind tunnel is discussed in Section 5 and some limitations of the work are highlighted. Suggestions for future research are also given. Finally, the conclusions are presented in Section 6.

2. Scaled Aircraft Flight Dynamics

The aircraft considered in this study is a 1/12th scaled BAe Hawk aircraft model shown in Figure 2 originally developed at Cranfield University [15,33] for dynamic wind tunnel testing. It has a fixed low-mounted main wing with wingspan of 780 mm fitted with ailerons, a single vertical tail fin and an all-moving, symmetric, horizontal tail stabilizer that is used for pitch control. It is attached to the end of the second manipulator arm via a gimbal (located in the cavity visible at the top of the fuselage), which can rotate in three directions, but here, it is constrained to pitch rotation only.

The flight dynamics model for the aircraft is described in this section, and is a fairly standard simplified model for a fixed-wing rigid-body aircraft; see, for example, [28,34]. Consider the aircraft flying wing-level in still air with negligible lateral perturbations. The motion is thus restricted to the 3-DOF longitudinal frame shown in Figure 3, where (u, w) is the pair of velocity components in the aircraft body frame with origin at the centre of gravity, θ is the pitch angle from the horizontal, V_T is the total air speed, α is the angle of attack, γ is the flight path angle, L is the lift force, D is the drag force, M is the pitch moment, $W = m_a g$ is the aircraft weight where m_a is the mass of the aircraft, g is the acceleration due to gravity, and T is the thrust.

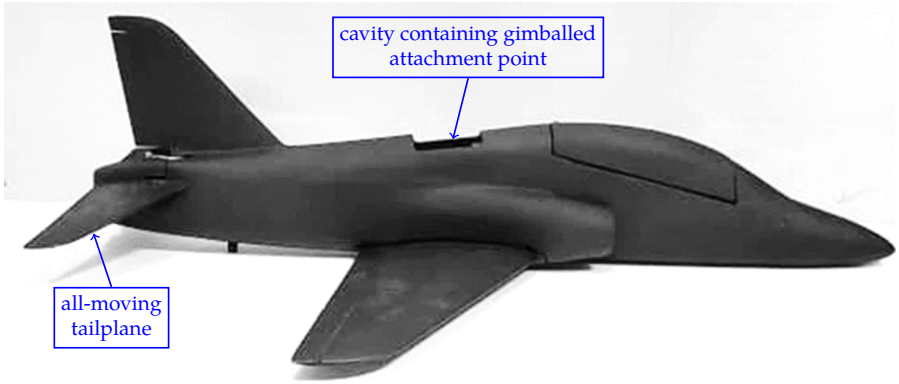


Figure 2. A 1/12th scaled BAe Hawk aircraft.

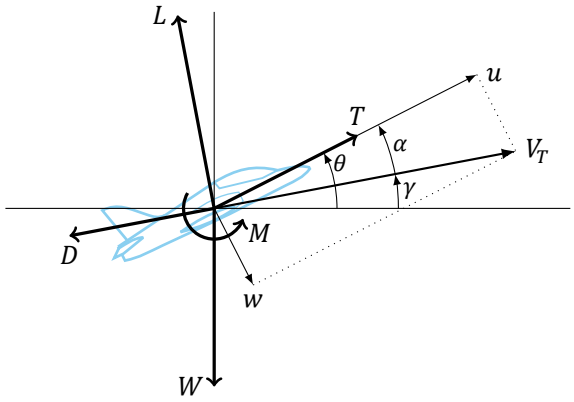


Figure 3. Configuration for 3-DOF aircraft longitudinal dynamics.

2.1. Aerodynamics

The lift, drag, and moment for the aircraft are, respectively,

$$L = \bar{q} S_w C_L, \qquad D = \bar{q} S_w C_D, \qquad M = \bar{q} S_w \bar{c}\, C_m, \tag{1}$$

where S_w is the wing area, $\bar{c}$ is the mean aerodynamic chord, C_L is the total lift coefficient, C_D is the drag coefficient, C_m is the pitch moment coefficient, and $\bar{q}$ is the dynamic pressure given by $\bar{q} = \frac{1}{2}\rho V_T^2$, where ρ is the density of air.

The total lift coefficient is given by [15,28]

$$C_L = C_{Lw} + \frac{S_t}{S_w} C_{Lt} \tag{2}$$

where C_{Lw} is the wing/body lift coefficient, C_{Lt} is the tail lift coefficient and S_t is the tailplane area. The body/wing lift coefficient is given by $C_{Lw} = C_{Lw\alpha}\alpha + C_{L0}$ where $C_{Lw\alpha}$ is the lift curve slope, α is the angle of attack, and C_{L0} is the lift coefficient at zero angle of attack. The tail lift coefficient is given by $C_{Lt} = C_{Lt\alpha}\,\alpha_t$, where $C_{Lt\alpha}$ is the tail lift curve slope, and α_t is the tailplane incidence given by $\alpha_t = \alpha - \varepsilon + \delta_t$ where δ_t is tailplane control angle and ε is the downwash angle at the tail. From [28],

$$\alpha - \varepsilon = \alpha\left(1 - \frac{\mathrm{d}\varepsilon}{\mathrm{d}\alpha}\right). \tag{3}$$

The drag coefficient C_D is given by

$$C_D = C_{D0} + \sigma C_L^2 \tag{4}$$

where C_{D0} is the drag coefficient at zero lift, and σ is the induced drag factor that can be calculated from $\sigma = 1/(\pi e AR)$ where e is the Oswald efficiency factor, and $AR = S_w/\bar{c}^2$ is the aspect ratio.

The pitch moment coefficient C_m is [28,34,35]

$$C_m = C_{m0} + C_{Lw}(h_{cg} - h_0) - \bar{V}_H\left(\frac{C_{Lt\alpha}}{C_{Lw\alpha}}C_{Lw}\left(1 - \frac{\mathrm{d}\varepsilon}{\mathrm{d}\alpha}\right) + C_{Lt\alpha}\delta_t\right) + \frac{\bar{c}}{2V_T}C_{mq}q \tag{5}$$

where C_{m0} is the initial pitch moment coefficient, C_{mq} is the pitch damping derivative, q is the pitch rate, h_{cg} is position of the centre of gravity, h_0 is the aerodynamic centre position, $\bar{c}$ is the mean aerodynamic chord, and $\bar{V}_H$ is tailplane volume coefficient, given by

$$\bar{V}_H = \frac{S_t l_t}{S_w \bar{c}} \tag{6}$$

where l_t is the tail moment arm.

2.2. Flight Dynamics

From Figure 3, the nonlinear flight dynamic equations of motion in the longitudinal plane are given (also see [28]) as

$$\begin{bmatrix} m_a\dot{u} + m_a q w \\ -m_a q u + m_a \dot{w} \\ \dot{q} I_y \end{bmatrix} = \begin{bmatrix} L\sin\alpha - D\cos\alpha + T - m_a g\sin\theta \\ -L\cos\alpha - D\sin\alpha + m_a g\cos\theta \\ M \end{bmatrix} \tag{7}$$

where $q = \dot{\theta}$ is the pitch rate and I_y is the moment of inertia about the body's y-axis.

From the still air assumption, the wind speed V_T and angle of attack α are related to the body velocities by

$$V_T = \sqrt{u^2 + w^2}, \tag{8}$$

$$\alpha = \mathrm{atan2}(w, u). \tag{9}$$

The velocity of the aircraft in the earth axes is given by

$$\begin{bmatrix} \dot{x}_e \\ \dot{h}_e \end{bmatrix} = \begin{bmatrix} \cos\theta & \sin\theta \\ \sin\theta & -\cos\theta \end{bmatrix}\begin{bmatrix} u \\ w \end{bmatrix}, \tag{10}$$

where (x_e, h_e) is the position in the earth axes.

From (5), the aircraft longitudinal trim (steady-state) condition can be derived as

$$\delta_{t_{trim}} = \frac{1}{\bar{V}_H C_{Lt\alpha}}\left(C_{m0} + C_{Lw}\left(h_{cg} - h_0\right)\right) - \frac{C_{Lw}}{C_{Lw\alpha}}\left(1 - \frac{d\varepsilon}{d\alpha}\right). \tag{11}$$

The trim angle of attack α and subsequent pitch, θ, and the thrust at trim can be calculated iteratively from (1)–(7).

3. Aircraft-Manipulator System Dynamics

A dynamic model of the aircraft-manipulator system (AMS) is required to simulate the system. The configuration is shown in Figure 4, whereby a 1/12th scaled BAe Hawk aircraft model is mounted onto the tip of a two-link revolute jointed manipulator via a joint that allows free pitch movement. The kinematics and dynamics of a two-link manipulator are well known, e.g., [36], and the extension to include the aircraft model is straightforward.

The horizontal axis is taken as x and the vertical (the height) is denoted as h. The first link has a length l_1 and mass m_1 with a centre of mass at the mid-point of the link and moment of inertia I_1. Similarly, the second link has a length l_2 and mass m_2 with a centre of mass at the mid-point of the link and moment of inertia I_2. The links are assumed to be

stiff and to have insignificant aerodynamic forces. There are servo motors attached to the first two joints that provide torques of τ_1 and τ_2 to control the joint angles θ_1 and θ_2. The joints are all assumed to be friction-free.

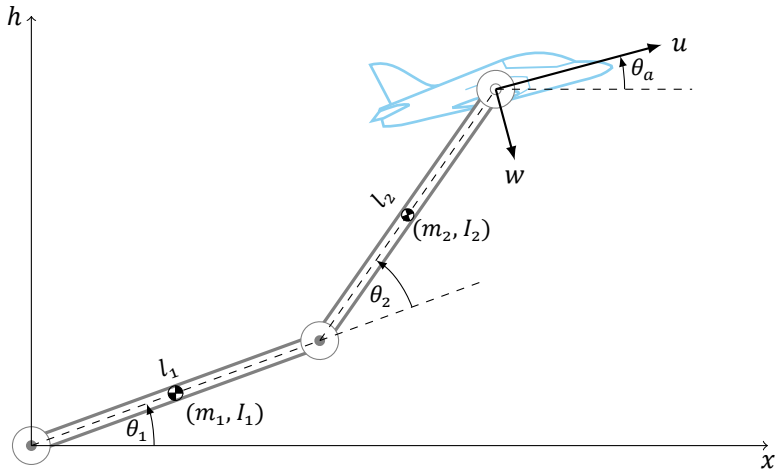


Figure 4. Manipulator aircraft system configuration.

A joint at the centre of mass of the aircraft model is attached to the tip of the second link. The aircraft joint is free to allow pitch rotation, and pitch angle with the horizontal is denoted by θ_a. The aircraft body velocity components u and w are shown, and the position of the aircraft (third joint) is denoted by (x_a, h_a).

3.1. Kinematics

The aircraft model position is related to the joint angles by

$$\begin{bmatrix} x_a \\ h_a \end{bmatrix} = \begin{bmatrix} l_1 \cos\theta_1 + l_2 \cos(\theta_1 + \theta_2) \\ l_1 \sin\theta_1 + l_2 \sin(\theta_1 + \theta_2) \end{bmatrix}, \tag{12}$$

with rates given by

$$\begin{bmatrix} \dot{x}_a \\ \dot{h}_a \end{bmatrix} = \begin{bmatrix} -l_1 \sin\theta_1 - l_2 \sin(\theta_1 + \theta_2) & -l_2 \sin(\theta_1 + \theta_2) \\ l_1 \cos\theta_1 + l_2 \cos(\theta_1 + \theta_2) & l_2 \cos(\theta_1 + \theta_2) \end{bmatrix} \begin{bmatrix} \dot{\theta}_1 \\ \dot{\theta}_2 \end{bmatrix}. \tag{13}$$

The inverse kinematics are well known, e.g., [36] (p. 30), and are given by

$$\theta_2 = \pm \operatorname{atan2}\left(\chi, x_a^2 + h_a^2 - l_1^2 - l_2^2\right), \tag{14}$$

where $\chi = \sqrt{(x_a^2 + h_a^2 + l_1^2 + l_2^2)^2 - 2\left[(x_a^2 + h_a^2)^2 + l_1^4 + l_2^4\right]}$ and

$$\theta_1 = \operatorname{atan2}(h_a, x_a) \mp \operatorname{atan2}\left(\chi, x_a^2 + h_a^2 + l_1^2 - l_2^2\right). \tag{15}$$

Note that for the wind tunnel configuration shown in Figure 4, generally the negative value of θ_2 is chosen (i.e., the elbow-up configuration) because this decreases the downwash aerodynamic effects of the links.

The angular rates are obtained from (13) as

$$\begin{bmatrix} \dot{\theta}_1 \\ \dot{\theta}_2 \end{bmatrix} = \frac{1}{d} \begin{bmatrix} l_2 \cos(\theta_1 + \theta_2) & l_2 \sin(\theta_1 + \theta_2) \\ -l_1 \cos\theta_1 - l_2 \cos(\theta_1 + \theta_2) & -l_1 \sin\theta_1 - l_2 \sin(\theta_1 + \theta_2) \end{bmatrix} \begin{bmatrix} \dot{x}_a \\ \dot{h}_a \end{bmatrix} \tag{16}$$

where the determinant $d = l_1 l_2 (\cos\theta_1 \sin(\theta_1 + \theta_2) - \sin\theta_1 \cos(\theta_1 + \theta_2))$.

3.2. Dynamics

Following the Lagrange modelling approach [36,37], we obtain the general open-chain dynamics system given by

$$\boldsymbol{\tau} = -\boldsymbol{\tau}_a + \mathbf{M}(\boldsymbol{\theta})\ddot{\boldsymbol{\theta}} + \mathbf{C}\left(\boldsymbol{\theta}, \dot{\boldsymbol{\theta}}\right)\dot{\boldsymbol{\theta}} + \mathbf{G}(\boldsymbol{\theta}) \tag{17}$$

where $\boldsymbol{\tau}$ is the net torque produced at the manipulator joints by the servomotors, $\boldsymbol{\tau}_a$ is the aerodynamic torque load produced by the aircraft, $\mathbf{M}$ is the generalised inertia matrix of each link, $\mathbf{C}$ is the matrix of Coriolis and centrifugal terms, and $\mathbf{G}$ is the gravitational effect on each link. The generalised inertia matrix is given by

$$\mathbf{M} = \begin{bmatrix} m_{11} & m_{12} & 0 \\ m_{21} & m_{22} & 0 \\ 0 & 0 & m_{33} \end{bmatrix} \tag{18}$$

where

$$m_{11} = m_1 l_1^2/4 + I_1 + m_2\left(l_1^2 + l_2^2/4 + l_1 l_2 \cos\theta_2\right) + I_2 + m_a\left(l_1^2 + l_2^2 + 2l_1 l_2 \cos\theta_2\right) + I_y, \tag{19}$$

$$m_{12} = m_2\left(l_2^2/4 + l_1 l_2/2 \cos\theta_2\right) + m_a\left(l_1 l_2 \cos\theta_2 + l_2^2\right), \tag{20}$$

$$m_{21} = m_{12}, \tag{21}$$

$$m_{22} = m_2 l_2^2/4 + I_2 + m_a l_2^2 + I_y, \tag{22}$$

$$m_{33} = I_y. \tag{23}$$

The matrix of Coriolis and centrifugal terms is given by

$$\mathbf{C}(\boldsymbol{\theta}, \dot{\boldsymbol{\theta}}) = c\begin{bmatrix} 2\dot{\theta}_2 & \dot{\theta}_2 & 0 \\ \dot{\theta}_1 & 0 & 0 \\ 0 & 0 & 0 \end{bmatrix} \tag{24}$$

where $c = -(m_2/2 + m_a) l_1 l_2 \sin\theta_2$, and the vector of gravitational terms is

$$\mathbf{g}(\boldsymbol{\theta}) = \begin{bmatrix} (m_1/2 + m_2 + m_a) l_1 g \cos\theta_1 \\ (m_2/2 + m_a) l_2 g \cos\theta_2 \\ 0 \end{bmatrix}. \tag{25}$$

The air velocity is the sum of the wind tunnel air speed V_{WT}, which acts horizontally, and the aircraft velocity $(\dot{x}_a, \dot{h}_a)$, as shown in Figure 5. Thus, the air velocity in free-flight and the wind tunnel are equated so that

$$\begin{bmatrix} \dot{x}_a \\ \dot{h}_a \end{bmatrix} = \begin{bmatrix} \dot{x}_e \\ \dot{h}_e \end{bmatrix} + \begin{bmatrix} -V_{WT} \\ 0 \end{bmatrix} \tag{26}$$

giving the airspeed on the aircraft in the wind tunnel as

$$V_T = \sqrt{(\dot{x}_a + V_{WT})^2 + \dot{h}_a^2}, \tag{27}$$

and angle of attack

$$\alpha = \theta_a - \text{atan2}(\dot{h}_a, \dot{x}_a + V_{WT}) \tag{28}$$

so that $\gamma = \theta_a - \alpha$. The aerodynamic forces are resolved to obtain the aerodynamic torque load:

$$\boldsymbol{\tau}_a = [\tau_{a1}, \tau_{a2}, \tau_{a3}]^T, \tag{29}$$

given by

$$\tau_{a1} = (L\cos\gamma - D\sin\gamma)(l_1\cos\theta_1 + l_2\cos\theta_2) + (L\sin\gamma + D\cos\gamma)(l_1\sin\theta_1 + l_2\sin\theta_2), \quad (30)$$

$$\tau_{a2} = (L\cos\gamma + D\sin\gamma)l_2\cos\theta_2 - (L\sin\gamma + D\cos\gamma)l_2\sin\theta_2, \quad (31)$$

$$\tau_{a3} = M. \quad (32)$$

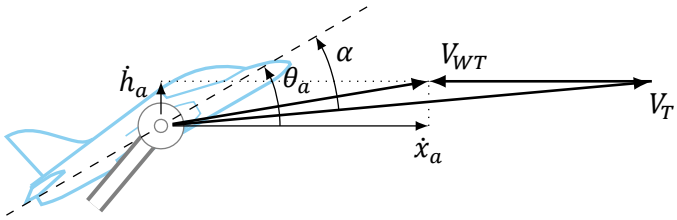


Figure 5. Air velocity as the sum of wind tunnel velocity and aircraft velocity.

3.3. Joint Control

The link joint angles, θ_1 and θ_2, are controlled via simple PID control, with the derivative action acting on the joint angular rates, $(\dot{\theta}_1, \dot{\theta}_2)$. The workspace of the manipulator is limited by the wind tunnel cross-section; thus, a linear controller works adequately well for the restricted range of angle demands. The joint angle reference commands, $(\theta_{\text{ref}\,1}, \theta_{\text{ref}\,2})$, are calculated from the inverse kinematics (14) and (15). Additional feedforward of the joint angular rate commands calculated from (16) is included. The controller outputs are the joint torques. It is assumed that the actuator and sensor dynamics are insignificant and can be ignored. Thus, the PID controllers are, for $i = 1, 2$,

$$\tau_i = k_{Pi}(\theta_{\text{ref}\,i} - \theta_i) + \int_0^t k_{Ii}(\theta_{\text{ref}\,i} - \theta_i)\mathrm{d}t + \tau_{\text{trim}\,i} + k_{Di}(\dot{\theta}_{\text{ref}\,i} - \dot{\theta}_i) \quad (33)$$

where $(k_{Pi}, k_{Ii}, k_{Di}), i = 1, 2$ are constant control gains and $\tau_{\text{trim}\,i}, i = 1, 2$ are the steady-state joint torques at the initial time, $t = 0$, calculated from the free-flight trim condition described in Section 2.2 and from (25)–(31). The control system architecture of each PID loop is shown in Figure 6.

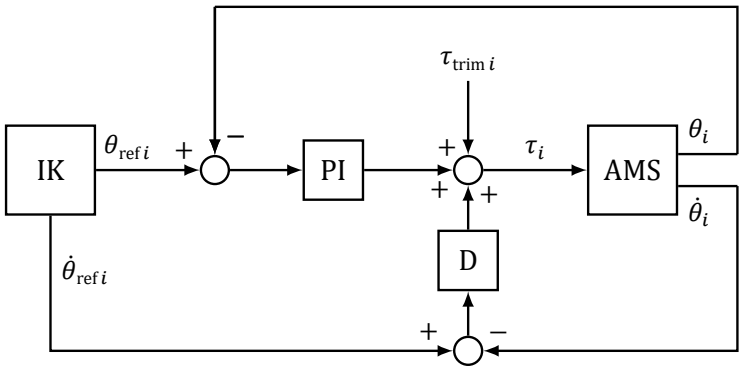


Figure 6. Block diagram showing system control architecture for the *i*th loop. The block denoted as IK represents the inverse kinematics' reference source.

4. Simulation

In order to demonstrate that the mechanism can replicate free-flight in the wind tunnel, a free-flight trajectory is simulated using the flight dynamics model of Section 2. From the inverse kinematics, the required angles and angular rates of the manipulator joints are calculated so that the aircraft in the wind tunnel experiences similar aerodynamic forces as the aircraft in the free-flight trajectory. These are passed to a simulation of the aircraft-manipulator system that is used to verify the system concept.

The equations are implemented in Simulink and the aircraft parameters are taken from [15,35] and are listed in Table 1. The controller gains were hand-tuned and are also given in Table 1. The codes for calculating the trim, the free-flight simulation, inverse kinematics, and AMS simulation are available on CORD—the Cranfield University Research Data repository [38].

Table 1. Aircraft and manipulator parameters.

Parameter	Symbol	Value	Units
Wing area	S_w	0.115	m^2
Mean aerodynamic chord	$\bar{c}$	0.161	m
Air density	ρ	1.2238	kg m^{-3}
Tailplane area	S_t	0.029	m^2
Wing body lift curve slope	$C_{Lw\alpha}$	3.72	rad^{-1}
Lift coefficient at zero α	C_{L0}	0.21	-
Tailplane lift curve slope	$C_{Lt\alpha}$	2.29	rad^{-1}
Oswald efficiency factor	e	0.70	-
Zero lift drag coefficient	C_{D0}	0.028	-
Initial pitch moment coefficient	C_{m0}	−0.050	-
Pitch damping derivative	C_q	−2.978	rad^{-1} s
Aerodynamic centre fraction	h_0	0.113	-
Centre of gravity fraction	h_{cg}	0.18	-
Tail moment arm	l_t	0.3656	m
Aircraft moment of inertia	I_y	0.219	kg m^2
Length of Link-1	l_1	0.32	m
Length of Link-2	l_2	0.32	m
Mass of Link-1	m_1	2.074	kg
Mass of Link-2	m_2	2.074	kg
Mass of aircraft	m_a	2.250	kg
Controller Gain P	$k_{Pi}, i = 1, 2$	100	N m rad^{-1}
Controller Gain I	$k_{Ii}, i = 1, 2$	4	N m rad^{-1} s^{-1}
Controller Gain D	$k_{Di}, i = 1, 2$	200	N m rad^{-1} s

The trajectory starts at trim at the wind tunnel airspeed of $V_T = 30$ m s^{-1}, an altitude of 10 m, and $g = 9.81$ ms^{-2}. The tail angle trim is calculated as $\delta_t = -0.0621$ rad (−3.56°), the pitch trim is $\theta_{\text{trim}\,a} = 0.0435$ rad (2.49°), and the thrust $T = 2.56$ N. A perturbation in both the pitch (and angle of attack) of 0.020 rad is applied at the initial condition and the free-flight simulation trajectory is recorded. Constant tail deflection angle and thrust of the trim values are also applied.

The resulting pitch response is shown in Figure 7 for the first 5 s, where the short period mode response can be observed, and for 60 s in Figure 8, where the phugoid mode response can be clearly observed.

The reference link angles are calculated via the inverse kinematics (13)–(15), with an initial position in the wind tunnel of $x_a = 0$ and $h_a = 0.40$ m. The initial joint torques are calculated as $\tau_{\text{trim}\,1} = -16.70$ Nm and $\tau_{\text{trim}\,2} = 2.058$ Nm. The AMS system is simulated from the same initial condition of the aircraft with the initial pitch perturbation in θ_a (and subsequent angle of attack perturbation, because the wind tunnel flow is horizontal). The resulting pitch response is also shown in Figure 7, where we can see that the response closely matches the free-flight response.

The aircraft height in the wind tunnel is shown in Figure 9, along with the free-flight altitude (translated to the wind tunnel axes). For the first second, the altitude deviations for the AMS response matches the free-flight closely. As the short period mode decays, the phugoid response starts to dominate, and the difference in the responses increases. The manipulator position controller does not follow the position exactly because of the natural phase lags in the system dynamics. The difference could be reduced by increasing the controller gains and by increasing the complexity of the controller so as to not excite the high-frequency dynamics.

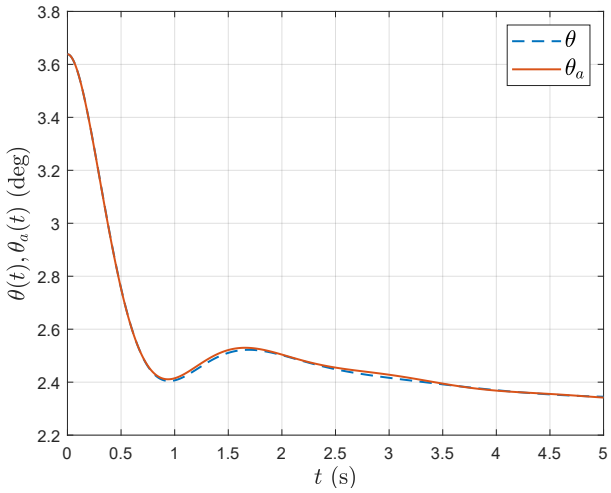


Figure 7. Short period mode pitch response of the free-flying Hawk model and the aircraft-manipulator system (AMS) model.

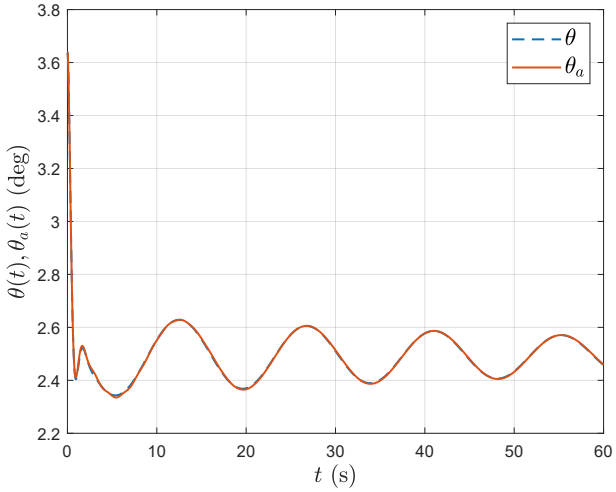


Figure 8. Phugoid mode pitch response of the free-flying Hawk model and the aircraft-manipulator system (AMS) model.

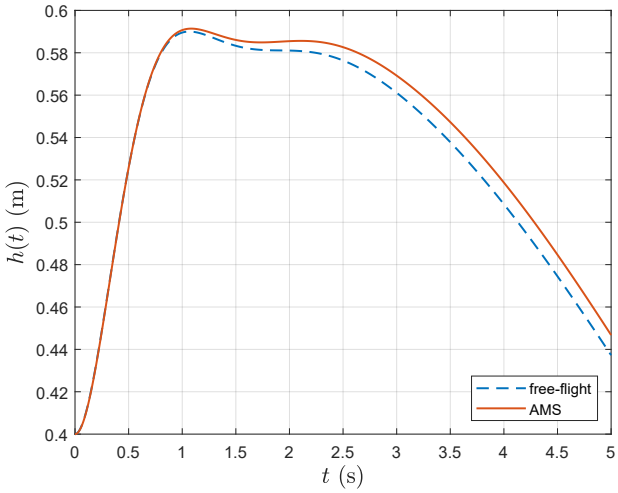


Figure 9. Short period mode altitude response of the free-flying Hawk model and the aircraft-manipulator system (AMS) model.

The altitude and horizontal positions relative to the air of the AMS simulation response are shown in Figure 10 along with the free-flight response resolved into the wind tunnel axes, that is, the response x_a calculated by integrating (26). The altitude deviation occupies nearly the entire wind tunnel working space (shown schematically in Figure 1). The altitude deviations in the AMS model response and the free-flight model response match well, but the surge distance matches less well.

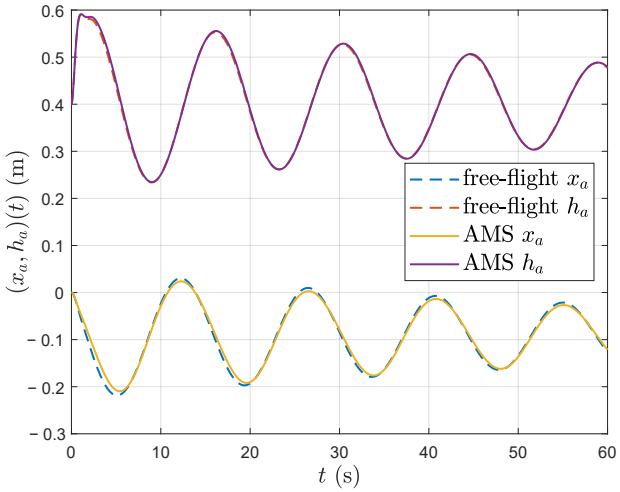


Figure 10. Phugoid mode height and lateral surge position response of the free-flying Hawk model (resolved into the wind tunnel axes) and the aircraft-manipulator system (AMS) model.

Figure 11 shows the response trajectory in the wind tunnel workspace. What can be clearly seen from Figure 11 is how the basic character of the phugoid response is reproduced. The interchange between kinetic and potential energies of the aircraft can be seen. As the aircraft climbs, it moves downstream in the wind tunnel as the speed falls, and as the height reduces due to reduced lift, the kinetic energy, and hence, speed, increases, and so the aircraft moves upstream.

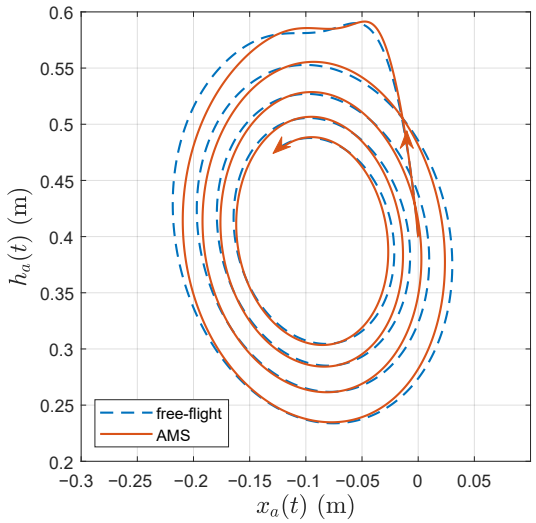


Figure 11. Phugoid mode position response of the aircraft-manipulator system (AMS) model in the wind tunnel.

5. Discussion

The results in the previous section show that the longitudinal free-flight motion can be replicated in a wind tunnel. In essence, what is happening is that the manipulator is providing the non-aerodynamic forces that a free-flying aircraft is exposed to, namely the

gravitational and thrust forces, that would otherwise be absent in a wind tunnel. This gives scope for variable thrust virtual flight as well as to artificially alter the gravitational force by means of the control so that flight in, for example, a Mars environment can be recreated. Of course, the system dynamics would require scaling with respect to the dynamic pressure to perform this. Hence, the control system should be improved to not only reduce errors, but to be designed so that the controller effectively cancels the manipulator dynamics whilst introducing the gravitational and thrust forces. This would mean that the AMS system could be viewed as 'dynamically equivalent' to the free-flight model in a similar manner to, for example, [39] or [40]. Control techniques to create a dynamically equivalent system could include model matching with feedback linearisation to cancel the manipulator dynamics. Robust sliding mode control is another potential candidate. This remains for future work, as do sensitivity and robustness studies to parametric uncertainty and unmodelled dynamics.

This study considers only the feasibility from a dynamics and control perspective. Prior to building a prototype, further work is also needed on the manipulator design, which needs to be performed with respect to not only the loads, but also the aerodynamic forces on the links and joints, the aeroelastic properties of the AMS, to ensure that the rig is sufficiently stiff and that it does not laterally deflect under load. The links require aerodynamic shaping to minimize the aerodynamic load and interference of the manipulator with the flow. In addition, for a closed return wind tunnel, the coupling of the aircraft dynamics and the disturbances on the recirculating flow should be investigated. Improvements to the aerodynamics model should also be made, to include, for example, the wing lift due to pitch rate, the dependence of the pitching moment on angle of attack, and the time delay between the wing and tail. Nonlinear aerodynamics such as stall could also improve the simulation model. Effects of lower wind tunnel velocity away from the centre line could also be modelled.

For classical aircraft configurations, the lateral and longitudinal dynamics are largely decoupled; hence, this study considers only the longitudinal dynamics. A similar rig could be proposed for lateral dynamics, which may be more useful because the dutch roll mode is more dependent on the aerodynamics than the phugoid mode. However, for flexible wing aircraft and some other configurations, the lateral and longitudinal coupling is significant; therefore, a full 6-DOF virtual flight test AMS should be designed and tested in the future.

The proposed AMS can be used for a number of applications. These include flight control algorithm testing, controller implementation testing, and aircraft-in-the-loop simulation. The flow in the wind tunnel is smooth, but in free-flight, aircraft often encounter gusts, turbulence, etc. A gust/turbulence generator could be inserted into the wind tunnel which would provide a cost-effective method to investigate its effect on the aircraft response. A tunnel with a good control of the airspeed could be used to increase the range of the surge variation; an analysis of this also remains for further work. This, of course, would rely on the wind tunnel speed having a sufficiently high bandwidth. The effect of the joint actuator dynamics and lags also remains for further work.

6. Conclusions

This paper proposes an aircraft-manipulator system that can replicate longitudinal free-flight in a wind tunnel. The system consists of a 1/12 scale model of a BAe Hawk attached to a 2-DOF manipulator via a pivot that allows free pitch rotation. Dynamic models of the aircraft in free-flight and of the AMS system are presented, and the feasibility of the system is investigated through simulation. The simulation results show that the proposed system can potentially provide a virtual flight test facility for longitudinal flight dynamics. The short period mode response of the aircraft is a consequence of the natural flight dynamic response of the aircraft, but the phugoid mode is imposed on the aircraft by determining the aircraft positions from a free-flight simulation response. This means that the constraints and interference of the phugoid dynamics on the aerodynamic response that would otherwise be imposed by constraining the phugoid motion of the aircraft are

removed, and the response in the wind tunnel is closer to the free response, than, for example, the 4-DOF Cranfield University rig briefly described in Section 1 [2,15,16,19].

Author Contributions: Conceptualisation, A.A.I. and J.F.W.; methodology, A.A.I. and J.F.W.; software, A.A.I. and J.F.W.; validation, A.A.I. and J.F.W.; formal analysis, A.A.I. and J.F.W.; investigation, A.A.I.; writing—original draft preparation, A.A.I.; writing—review and editing, J.F.W. and G.T.; supervision, J.F.W. and G.T. All authors have read and agreed to the published version of the manuscript.

Funding: This research is partly funded by the Tertiary Educational Trust Fund (TETFUND) Nigeria, grant number TETF/ES/UNIV/OGUNSTATE/TSAS/2020. https://tetfund.gov.ng/index.php/guideline-4/ (accessed on 17 October 2024).

Institutional Review Board Statement: Not applicable.

Informed Consent Statement: Not applicable.

Data Availability Statement: The codes for calculating the trim, the free-flight simulation, inverse kinematics, and AMS simulation are on CORD—the Cranfield University research data repository doi:tbc, url: https://dspace.lib.cranfield.ac.uk/handle/1826/20712 (accessed on 17 October 2024). A Hawk CAD model is available on request from the corresponding author.

Acknowledgments: Acknowledgements to Simon Prince, Pavithra Kasula, and Elzbieta Jarzębowska for their contributions to the development and assessing the aerodynamic feasibility of the model in the wind tunnel.

Conflicts of Interest: The authors declare no conflicts of interest. The funders had no role in the design of the study; in the collection, analyses, or interpretation of data; in the writing of the manuscript; or in the decision to publish the results.

Abbreviations

The following abbreviations are used in this manuscript:

AMS	Aircraft-Manipulator System
DOF	Degrees Of Freedom
PID	Proportional Integral Derivative

References

1. Greenwell, D.I. A review of unsteady aerodynamic modelling for flight dynamics of manoeuvrable aircraft. In Proceedings of the AIAA Atmospheric Flight Mechanics Conference and Exhibit, Providence, RI, USA, 16–19 August 2004; Number AIAA 2004-5276. [CrossRef]
2. Cook, M.V. On the use of small scale aircraft models for dynamic wind tunnel investigation of stability and control. *Trans. Inst. Meas. Control* **1987**, *9*, 190–197. [CrossRef]
3. Huang, M.; Wang, Z.W. Review of wind tunnel based virtual flight testing techniques for evaluation of flight control systems. *Int. J. Aerosp. Eng.* **2015**, *2015*, 15. [CrossRef]
4. Malvestuto, F.S.; Gale, L.J.; Wood, J.H. *Compilation of Test Data on 111 Free-Spinning Airplane Models Tested in the Langley 15-Foot and 20-Foot Free-Spinning Tunnels*; NASA: Washington, DC, USA, 1947; Research Memorandum NACA-RM-L7E1: 20090025259, NACA.
5. Golovkin, M.A.; Efremov, A.A.; Kritskii, B.S.; Pavlenko, O.V.; Tsipenko, V.G. To the estimation of force and pitching moment coefficients acting on the model, full-scale aircraft and their elements at supercritical angles of attack and in a spin. *Russ. Aeronaut.* **2020**, *63*, 643–651. [CrossRef]
6. Manning, T.E.; Ratliff, C.L.; Marquart, E.J. Bridging the gap between ground and flight tests: Virtual flight testing (VFT). In Proceedings of the 1st AIAA Aircraft Engineering, Technology and Operations Congress, Los Angele, CA, USA, 19–21 September 1995; Number AIAA-95-3875. [CrossRef]
7. Ignatyev, D.D.; Sidoryuk, M.E.; Kolinko, K.A.; Khrabrov, A.N. Dynamic rig for validation of control algorithms at high angles of attack. *J. Aircr.* **2017**, *54*, 1760–1771. [CrossRef]
8. Guo, L.; Zhu, M.; Nie, B.; Kong, P.; Zhong, C. Initial virtual flight test for a dynamically similar aircraft model with control augmentation system. *Chin. J. Aeronaut.* **2017**, *30*, 602–610. [CrossRef]
9. Huang, M.; Wang, Z.W.; Guo, Z.Y.; Niu, Y.B. Design of the wind tunnel based virtual flight testing evaluation method for flight control systems. *Proc. Inst. Mech. Eng. Part G J. Aerosp. Eng.* **2018**, *232*, 17–29. [CrossRef]

10. Lu, S.; Wang, J.; Wang, Y. Research on similarity criteria of virtual flight test in low-speed wind tunnel. In Proceedings of the IEEE International Conference on Power, Intelligent Computing and Systems (ICPICS 2021), Shenyang, China, 29–31 July 2021; pp. 121–126. [CrossRef]
11. Tai, S.; Wang, L.; Yue, T.; Liu, H. Test Data Processing of Fly-by-Wire Civil Aircraft in Low-Speed Wind Tunnel Virtual Flight. In Proceedings of the 12th International Conference on Mechanical and Aerospace Engineering (ICMAE 2021), Athens, Greece, 16–19 July 2021; pp. 96–101. [CrossRef]
12. Fu, J.; Shi, Z.; Gong, Z.; Lowenberg, M.H.; Wu, D.; Pan, L. Virtual flight test techniques to predict a blended-wing-body aircraft in-flight departure characteristics. *Chin. J. Aeronaut.* **2022**, *35*, 215–225. [CrossRef]
13. Zhang, L.; Huang, Y.; Zhu, Z.; Gao, L.; Chen, F.; Wu, F.; He, M. Virtual flight test of pitch and roll attitude control based on circulation control of tailless flying wing aircraft without rudders. *Chin. J. Aeronaut.* **2023**, *36*, 52–62. [CrossRef]
14. Tai, S.; Wang, L.; Wang, Y.; Bu, C.; Yue, T. Flight dynamics modeling and aerodynamic parameter identification of four-degree-of-freedom virtual flight test. *AIAA J.* **2023**, *61*, 2652–2665. [CrossRef]
15. Hinds, H.A. The Application of a Modified Stepwise Regression (MSR) Method to the Estimation of Aircraft Stability and Control Derivatives. Ph.D. Thesis, Cranfield University, Bedford, UK, 1996.
16. Carnduff, S.D.; Erbsloeh, S.D.; Cooke, A.K.; Cook, M.V. Characterizing stability and control of subscale aircraft from wind-tunnel dynamic motion. *J. Aircr.* **2009**, *46*, 137–147. [CrossRef]
17. Pattinson, J.; Lowenberg, M.H.; Goman, M.G. Investigation of poststall pitch oscillations of an aircraft wind-tunnel model. *J. Aircr.* **2013**, *50*, 1843–1855. [CrossRef]
18. Gong, Z.; Araujo-Estrada, S.; Lowenberg, M.H.; Neild, S.A.; Goman, M.G. Experimental investigation of aerodynamic hysteresis using a five-degree-of-freedom wind-tunnel maneuver rig. *J. Aircr.* **2019**, *56*, 1029–1039. [CrossRef]
19. Pontillo, A.; Yusuf, S.; Lopez, G.; Rennie, D.; Lone, M. Investigating pitching moment stall through dynamic wind tunnel test. *Proc. Inst. Mech. Eng. Part G J. Aerosp. Eng.* **2020**, *232*, 267–279. [CrossRef]
20. Asai, K.; Konno, A.; Jiang, X.; Numata, D.; Abe, H.; Nakata, N.; Hara, T. Multi-degree-of-freedom dynamic wind-tunnel testing of a delta wing using a robotic manipulator. In Proceedings of the 28th Congress of the International Council of the Aeronautical Sciences (ICAS 2012), Brisbane, Australia, 23–28 September 2012; Number ICAS2012-3.1ST2.
21. Wei, R.; Che, B.H.; Sun, C.B.; Zhang, J.; Lu, Y.Q. A three degree of freedom manipulator used for store separation wind tunnel test. *IOP Conf. Ser. Mater. Sci. Eng.* **2018**, *372*, 012035. [CrossRef]
22. Davison, P.M.; Lowenberg, M.H.; Bernardo, M. Experimental analysis and modeling of limit cycles in a dynamic wind-tunnel rig. *J. Aircr.* **2003**, *40*, 776–785. [CrossRef]
23. Navaratna, P.D.B.; Lowenberg, M.H.; Neild, S.A. Minimally constrained flight simulation in wind tunnel. *J. Aircr.* **2019**, *56*, 1353–1366. [CrossRef]
24. Pattinson, J.; Lowenberg, M.H.; Goman, M.G. Multi-degree-of-freedom wind-tunnel maneuver rig for dynamic simulation and aerodynamic model identification. *J. Aircr.* **2013**, *50*, 551–566. [CrossRef]
25. Wang, X.; Peng, M.; Hu, Z.; Chen, Y.; Lin, Q. Feasibility investigation of large-scale model suspended by cable-driven parallel robot in hypersonic wind tunnel test. *Proc. Inst. Mech. Eng. Part G J. Aerosp. Eng.* **2017**, *231*, 2375–2383. [CrossRef]
26. Ji, Y.; Peng, M.; Lin, Q.; Yin, C. Wire-driven parallel robot suspension system for SDM in a low-speed wind tunnel. *Adv. Mech. Eng.* **2023**, *15*, 16878132231170262. [CrossRef]
27. Ahmadi, M.; Guigue, A.; Gibeault, M.; Tang, F.C. Mechatronic design of redundant robotic systems for captive trajectory simulation applications. In Proceedings of the 10th IASTED International Conference on Control and Applications (CA 2008), Quebec City, QC, Canada, 26–28 May 2008; pp. 24–29.
28. Cook, M. *Flight Dynamics Principles—A Linear Systems Approach to Aircraft Stability and Control*, 3rd ed.; Butterworth-Heinemann: Oxford, UK, 2013. [CrossRef]
29. Sinha, N.K.; Ananthkrishnan, N. *Elementary Flight Dynamics with an Introduction to Bifurcation and Continuation Methods*; CRC Press: Boca Raton, FL, USA, 2013.
30. Stengel, R.F. *Flight Dynamics*; Princeton University Press: Princeton, NJ, USA, 2004.
31. Whidborne, J.F.; Jarzębowska, E.; Agarwal, V.; Ishola, A.A. Manipulator-aircraft dynamical system dedicated for wind tunnel testing. In Proceedings of the 16th Conference on Dynamical Systems—Theory and Applications (DSTA 2021), Lódź, Poland, 6–9 December 2021; Awrejcewicz, J., Kaźmierczak, M., Mrozowski, M., Olejnik, P., Eds.; Lodz University of Technology Press: Lodz, Poland, 2021; pp. 115–116. [CrossRef]
32. Ishola, A.A.; Whidborne, J.F.; Kasula, P. Control for novel 3-DOF flight testing in a wind tunnel. In Proceedings of the 14th UKACC International Conference on Control (CONTROL 2024), Winchester, UK, 10–12 April 2024; pp. 321–322. [CrossRef]
33. Malik, I.A. The Design, Development and Evaluation of an Active Control Aircraft Model Wind Tunnel Facility. Ph.D. Thesis, Cranfield University, Bedford, UK, 1982.
34. Stevens, B.L.; Lewis, F.L. *Aircraft Control and Simulation*, 2nd ed.; John Wiley: Hoboken, NJ, USA, 2003. [CrossRef]
35. O'Gorman, D. Flight Dynamics Modelling of a 4 Degrees-of-Freedom Dynamic Test Rig. Master's Thesis, Cranfield University, Bedford, UK, 2006.
36. Yoshikawa, T. *Foundations of Robotics—Analysis and Control*; MIT Press: Cambridge, MA, USA, 1990. [CrossRef]
37. Žefran, M.; Bullo, F. Langrangian Dynamics. In *Robotics and Automation Handbook*, 1st ed.; Kurfess, T.R., Ed.; CRC Press: Boca Raton, FL, USA, 2005; Chapter 5. [CrossRef]

38. Whidborne, J.; Tang, G.; Ishola, A. *Code—Nonlinear Dynamics and Control of a Novel 3-DOF Aircraft-Manipulator for Dynamic Wind Tunnel Tests*; Cranfield Online Research Data (CORD) Repository: Bedford, UK, 2024. [CrossRef]
39. Liang, B.and Xu, Y.; Bergerman, M. Mapping a space manipulator to a dynamically equivalent manipulator. *J. Dyn. Syst. Meas. Control* **1998**, *120*, 1–7. [CrossRef]
40. Jarzębowska, E.; Kłak, M. Quaternion-based spacecraft dynamic modeling and reorientation control using the dynamically equivalent manipulator approach. In *Advances in Spacecraft Attitude Control*; Sands, T., Ed.; IntechOpen: Rijeka, Croatia, 2020; Chapter 3. [CrossRef]

Disclaimer/Publisher's Note: The statements, opinions and data contained in all publications are solely those of the individual author(s) and contributor(s) and not of MDPI and/or the editor(s). MDPI and/or the editor(s) disclaim responsibility for any injury to people or property resulting from any ideas, methods, instructions or products referred to in the content.



https://dspace.org/

An aircraft-manipulator system for virtual flight testing of longitudinal flight dynamics

Ishola, Ademayowa A.; Whidborne, James F.; Tang, Gilbert

2024-12-01
MDPI
https://doi.org/10.3390/robotics13120179
Ishola AA, Whidborne JF, Tang G. (2024) An aircraft-manipulator system for virtual flight testing of longitudinal flight dynamics. Robotics, Volume 13, Issue 12, December 2024, Article number 179

Downloaded from a DSpace repository. https://dspace.org/